NASA TECHNICAL NOTE

NASA TN D-5012

REACTIVITY CHANGES OF A FAST REACTOR CORE DUE TO ELASTIC-PLASTIC STRAIN AND CREEP

by Richard L. Puthoff

Lewis Research Center

Cleveland, Ohio

NATIONAL AERONAUTICS AND SPACE ADMINISTRATION • WASHINGTON, D. C. • JANUARY 1969

NASA TN D-5012

REACTIVITY CHANGES OF A FAST REACTOR CORE DUE TO ELASTIC-PLASTIC STRAIN AND CREEP

By Richard L. Puthoff

Lewis Research Center
Cleveland, Ohio

NATIONAL AERONAUTICS AND SPACE ADMINISTRATION

For sale by the Clearinghouse for Federal Scientific and Technical Information
Springfield, Virginia 22151 – CFSTI price $3.00

ABSTRACT

An elastic-plastic and creep analysis which predicts the actual core movement during the reactor operation and determines corresponding reactivity change is presented. A transport code was used for determining core reactivity. A reference design is included to aid in applying the analysis. The design consists of a 12-inch (30.48-cm) core containing $U^{233}O_2$ fuel surrounded by a 4-inch- (10.16-cm-) thick tungsten reflector. A reactivity decrease of -$3.85 resulted during the heating period with further reactivity decreases of -$0.06 during the first 90 hours and -$0.05 between 90 and 2000 hours.

REACTIVITY CHANGES OF A FAST REACTOR CORE DUE TO ELASTIC-PLASTIC STRAIN AND CREEP

by Richard L. Puthoff

Lewis Research Center

SUMMARY

In space power applications small nuclear reactors with core diameters of 12 inches (30.48 cm) and less are encountered. Such small diameters result in high neutron leakage at the outer boundaries. Structural dimensional changes, such as fuel-rod bowing in the core, can have a pronounced effect on the neutron leakage and, hence, on the core reactivity. Often these effects are analyzed by making arbitrary movements of the core and calculating the subsequent reactivity change.

This report presents an elastic-plastic and creep analysis which predicts the actual core movement during the reactor operation. This analysis uses the same equilibrium and compatibility equations as an elastic problem, but combines these equations with nonlinear stress-strain equations for the plastic regime. The resulting equations are solved by the use of the method of successive approximations.

A reference design is included to aid in applying the analysis. The design incorporates hexagon fuel elements, with central coolant passages, bundled together with band straps to prevent fuel bowing. The fuel is fully enriched uranium dioxide ($U^{233}O_2$) mixed 40 volume percent in a tungsten carrier. The core has a diameter and length of 12 inches (30.48 cm) and is surrounded radially and axially by a 4-inch- (10.16-cm-) thick tungsten reflector.

Core movements of the reference design were determined, and corresponding reactivity changes were calculated by a transport code for the following situations:

(1) Cold to hot fuel power, -$3.85

(2) Ninety hours of operation, -$0.06

(3) Ninety to 2000 hours of operation, -$0.05

Due to the immediate relaxation of stresses, however, anytime the reactor is brought to full power, high residual stresses will occur upon chilldown.

INTRODUCTION

Nuclear reactors are being considered as a potential source of energy for many space power applications. These include auxiliary electric power generation systems using a Rankine or Brayton cycle for energy conversion. The use of these cycles, however, requires heat exchangers or radiators which place a premium on the requirements for a low weight, high power density, high temperature capability reactor. The reactor which meets this requirement is the fast reactor containing a high-temperature cermet.

In designing a fast core, the small diameters associated with this type of reactor result in high neutron leakage at the outer boundaries. Indeed, this leakage has been used as a method for controlling fast reactors. In this method drums containing a neutron reflector material are rotated in and out of the boundary flux, thus affecting the reactivity of the core. By the same token, if control is possible in this manner, structural dimensional changes can also affect the reactivity of the core.

Reactivity effects due to dimensional changes of a liquid-metal-cooled fast reactor were first discovered in Experimental Breeder Reactor I (EBR I) loadings Mark I and Mark II when bowing of the fuel elements occurred (ref. 1). This core consisted of fuel rods, with sufficient clearance between the rods to permit lateral movement. When a fission distribution occurs across the core, the heat-generation rate in any particular rod is highest closest to the center of the core. This condition results in a temperature gradient within the rod, and, consequently, bowing in the inward direction occurs. With the Mark I and Mark II loadings, this inward bowing led to a positive reactivity contribution with ensuing stability problems.

The Jet Propulsion Laboratory has conducted a study of the reactivity effects from fuel displacement in small thermionic fast reactors (ref. 2). The core was 17 centimeters in radius, liquid-metal-cooled, and developed a thermal power applicable to a 50- to 100-kilowatt-electric thermionic system. Arbitrary movements were made in the core and their effects studied. In one case, for example, the whole core was uniformly compressed radially 1 millimeter, and the surrounding outer regions were correspondingly moved inward without compression. The effect of this change on core reactivity was large and positive, over the prompt criticality threshold of $1.

In a recent study by R. Sullivan of Lewis Research Center (ref. 3), highly fueled, lithium-cooled fast reactors of various sizes and designs (9- to 21-cm radius, beryllium and tungsten reflected) were analyzed with respect to reactivity changes as a result of core movement. This core analysis was two-dimensional and included both radial and axial zones. Changes in physical dimensions were made in various zones or combination of zones to simulate fuel bowing in unconstrained fuel elements. The effects on reactivity change were significant. Reactivity increases greater than $4 were calculated.

Many studies of reactivity changes in fast cores have merely evaluated the effect of

arbitrary movements of core regions to simulate change. This method was necessary, for in many designs consisting of bulkheads and spacers, analysis becomes difficult. Further, for high-temperature cermets with high fuel loadings common in fast reactors, material property data has been scarce and often unreliable. These studies, however, did show a need both to prevent fuel-rod bowing and to be able to analytically predict core movements and subsequent reactivity changes.

With continuing research in high-temperature cermet material, more data are becoming available to predict structural behavior under loads at high temperatures and high fuel loadings (appendix A). Therefore, the intent of this report is to present an elastic-plastic and creep analysis for predicting the actual core movement and subsequent reactivity changes due to the stresses and strains of the reactor during operation. For application of the analysis a reference design is presented of a fast liquid-metal-cooled reactor in which the fuel elements are banded together to prevent fuel bowing and to provide close contact during any core movement. Strains are calculated for nonuniform volumetric expansion of the core due to initial heating and a radial temperature gradient. Although the design presented is small and compact, the elastic-plastic analysis used is general enough in principle to be applied to other size reactor systems providing there is close contact throughout the core.

SYMBOLS

A area, $in.^2$; cm^2

A_0 internal heat-generation rate, $Btu/(hr)(in.^3)$; W/m^3

A_1 creep constant

a radius, in.; cm

b radius, in.; cm

C_p specific heat at constant pressure, $Btu/(lb)(^oF)$; $J/(kg)(K)$

C_1 integration constant

C_2 integration constant

d diameter, in.; cm

E modulus of elasticity, psi; N/m^2

h heat-transfer coefficient, $Btu/(ft^2)(hr)(^oF)$; $W/(m^2)(K)$

J number of data points

K thermal conductivity, $Btu/(ft)(hr)(^oF)$; $W/(cm)(^oC)$

k_{eff} effective multiplication factor

N	creep exponent
Nu	Nusselt number
n	number of axial (or radial) stations
P	pressure load on core outside diameter, psi; N/m^2
P_0	first term of Legendre expansion, corresponds to isotropic neutron scattering distribution
Pr	Prandtl number
Q	total heat transferred, Btu/hr; W
ΔQ	total heat transferred in incremental length, Btu/hr; W
Q/A	heat flux, Btu/(hr)(ft^2); W/m^2
R	residual
Re_d	Reynolds number
r	radius, in.; cm
S	side of hexagon, in.; cm
S_2	acronym designating low-order discrete angular segmentation method for solving the transport equation
T	time, hr
ΔT	time increment, hr; sec
t	temperature, ^oF; K
Δt	total coolant temperature rise, ^oF; K
t_a	temperature at radius a, ^oF; K
t_b	temperature at radius b, ^oF; K
t_f	temperature at film, ^oF; K
V	velocity, ft/sec; cm/sec
$\Delta V/V$	volume change, percent
W	mass flow, lb/hr; kg/sec
Δx	incremental length, in.; cm
α	coefficient of thermal expansion, in./in./^oF; cm/cm/K
β	delayed neutrons
ϵ	rate of strain, in./in./hr; cm/cm/sec

$\Delta\epsilon$ incremental strain, in./in.; cm/cm

$\Delta\epsilon_{ec}$ equivalent creep strain, in./in.; cm/cm

ϵ_{et} equivalent total strain, in./in.; cm/cm

ϵ_p equivalent plastic strain, in./in.; cm/cm

ϵ_r radial strain, in./in.; cm/cm

$\Delta\epsilon_r$ incremental radial strain, in./in.; cm/cm

ϵ_z longitudinal strain, in./in.; cm/cm

$\Delta\epsilon_z$ incremental longitudinal strain, in./in.; cm/cm

ϵ_θ tangential strain, in./in.; cm/cm

$\Delta\epsilon_\theta$ incremental tangential strain, in./in.; cm/cm

μ Poisson's ratio

μ_1 absolute viscosity, lb/(ft)(hr); (N)(sec)/m^2

ρ density, lb/ft^3; kg/m^3

σ_e equivalent stress, psi; N/m^2

σ_r radial stress, psi; N/m^2

σ_z longitudinal stress, psi; N/m^2

σ_θ tangential stress, psi; N/m^2

\$ unit of reactivity; dollar is equal to a reactivity of β

Subscripts:

i axial stations

n radial stations

Superscripts:

c creep

gr radiation growth

p plastic flow

sw radiation swelling

METHOD OF CORE ANALYSIS

The fast reactor is characterized by its high neutron flux, large boundary leakage, and small diameters. Multimegawatt reactors often have core diameters less than 12 inches (30.48 cm). With a length to diameter ratio of 1, these cores are quite small and compact.

In figure 1 a reactor design is presented in which the core, consisting of hexagonal

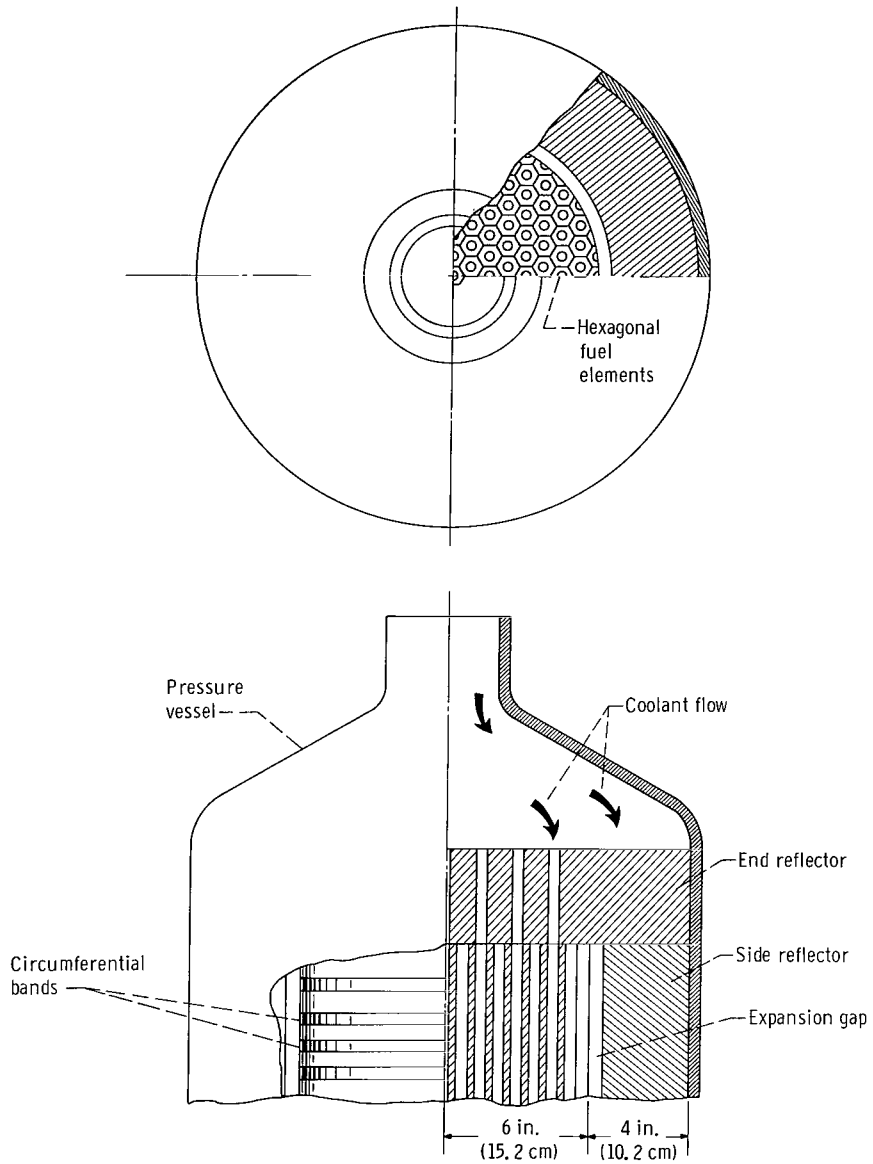

Figure 1. - Fast reactor with 12-inch (30.48-cm) core.

fuel elements, is surrounded radially and axially by 4 inches (10.16 cm) of reflector and then contained in a pressure vessel. The hexagonal fuel elements have a central passage for the coolant. They are bundled together tightly by circumferential bands (see fig. 1). During the reactor operation these bands would be in yield, so that a relatively constant load of 500 psi (344 N/cm^2) would be applied to the assembly. Between the core and reflectors are expansion gaps to allow unobstructive movement of the core. Thus, expansion occurs radially and axially. In the axial direction, however, the core is attached at the inlet and allowed to expand only toward the outlet.

This design will prevent fuel bowing as all the hexagonal elements are in contact with each other due to a predesigned radial compressive load. The Mark III loading of EBR I (ref. 1), in a similar concept, incorporated a clamping arrangement to ensure tightness of the subassemblies and thus prevent the fuel bowing that occurred in the Mark I and II loadings.

The thermal gradients still exist, however, and now, in addition, a radial boundary load has been applied. The loads cause stresses and strains, and strains are core movements. The question to be answered is whether these gross strains and subsequent reactivity changes are as detrimental as the occurrence of individual fuel bowing.

Due to its compact size and the bundling of the fuel elements, the core design of figure 1 can be considered as a homogeneous solid cylinder with a boundary load at the outer radius. This design lends itself well for calculating core criticality and flux shapes by the transport theory using a two-dimensional cylindrical geometry. The computations for plastic flow and creep can utilize the method of successive approximations originally applied to the study of stresses in rotating machinery and redeveloped in reference 4 for application to a reactor core (cylindrical geometry).

Neutronic Analysis

In the energy range of fast-reactor spectra the variations of cross sections with energy are sufficiently large so that bulk treatment of large energy regions, such as the use of the four-factor formula (ref. 5), is not practiced. Therefore, methods of multigroup solutions of transport or diffusion equations must be used. In addition, as the dimensions of the fast reactor core become smaller and approach an appreciable percentage of the distance of a neutron mean free path, transport solutions are required. Even in large fast-reactor systems, the transport solution provides a more precise calculation (ref. 6).

Solutions of multiregion-multigroup equations require the use of high-speed digital computers. There are many codes available for application to a fast reactor of this size. The code used in the analysis of this report is a two-dimensional discrete angular segmentation transport program (ref. 7) (hereinafter referred to as TDSN). It is a numerical, iterative finite difference method in which the continuous angular distribution of neutron velocities is represented by considering discrete angular directions.

A P_0 approximation for neutron scattering and a S_2 discrete angle approximation were used for the neutronic calculations of this report. Seven group cross sections were obtained from the Gam II program (ref. 8) which averaged the cross sections over the energy spectrum resulting from the interaction of the fission neutrons with the core and reflector material. As core growth occurred, the core composition remained the same, and the macroscopic densities were adjusted. All transport calculations were performed

using the two-dimensional cylindrical geometry option. The output of the transport program provides the core multiplication factor k_{eff}, integrated power ratio, and the flux shapes for each energy group.

Heat-Transfer Analysis

Before the core stresses and strains are calculated, the power ratios of the reactor must be converted into a temperature map. For liquid-metal cores, the convection heat-transfer coefficient can be considered as constant over small velocity and temperature ranges, thus simplifying the calculations. Appendix B contains the derivations of the heat-transfer equations that are applied to the calculations of this report.

Stress-Strain Analysis

When the core is considered to be homogeneous with a temperature profile in the radial direction (at a given axial location) and a boundary force at the outer radius, the solution lends itself well to conventional elastic cylindrical geometry methods. In nuclear reactor applications, however, the high temperatures of operation necessitate using the maximum load-carrying capacity of the materials. Therefore, the materials may be operated beyond the elastic range into the plastic regime.

The solution of plastic flow problems involves the use of the same equilibrium and compatibility equations as elasticity problems, but these equations must be combined with nonlinear stress-strain relations instead of the linear Hooke's law. In many applications, however, the resulting equations are solved in the same manner as the elasticity equations, except that a certain amount of systematic trial-and-error manipulation is required. Such a method has been used by Millenson and Manson (ref. 9) in connection with the rotating disk, but the approach is general and can be used for other problems as well. It is, in fact, ideally suitable to reactor core analysis. In similar work, analyses of a reactor pressure vessel (ref. 10) and a hollow fuel element (ref. 11), the method of successive approximations was used for the plastic flow calculations.

The successive approximations method was also chosen for its potential. It can be applied to creep problems (outlined in the next section) and cyclic stress problems (ref. 12). It offers a solution in which the strains (and core growth) are dependent on the history of reactor operation.

The derivation of equations and the method of calculation for a homogeneous reactor core (cylindrical geometry) are presented in reference 4.

Creep Analysis

Creep may be calculated in the same manner as plastic flow, that is, by the method of successive approximations. In creep, however, the strain path becomes time dependent. The relation between the strain and time is expressed by three basic laws, the time-hardening, strain-hardening, and life-fraction rules. For this report the time-hardening rule has been arbitrarily used (ref. 13).

The shape of the strain against time curve at load is divided into primary, secondary, and tertiary. The creep then becomes the slope of the curve at any point. This analysis considers only secondary creep, which is the major operating regime. There are many stress-strain - time relations to choose from (ref. 14); however, the final one chosen is often dependent upon the data available.

The derivation of the creep equations and the method of calculation used for a homogeneous reactor core (cylindrical geometry) is presented in reference 4. The stress-strain - time relation used in this analysis is presented in appendix C.

Additional Applications

In a reactor core, in addition to the thermal effects, there are radiation effects on the fuel material. These effects are irradiation growth and irradiation swelling (ref. 15). The growth of a single uranium crystal as a result of irradiation is known as irradiation growth, while irradiation swelling is volumetric instability caused by the fission products produced by the fuel.

As fast-reactor cores are designed for long lifetimes (10 000 hr), this irradiation growth must be taken into consideration. To interpret the theoretical mechanisms of irradiation growth and express them in a differential form for a stress-strain analysis would be quite difficult. However, it is considerably simpler to factor actual test data into the successive approximation method in finite difference form by utilizing a high speed computer.

From experimental data the growth strains of swelling and irradiation are introduced into the analysis, along with creep, as follows:

$$\epsilon_r = \frac{1}{E}\left[\sigma_r - \mu(\sigma_\theta + \sigma_z)\right] + \alpha T + \epsilon_r^c + \epsilon_r^{gr} + \epsilon_r^{sw} + \Delta\epsilon_r^c + \Delta\epsilon_r^{gr} + \Delta\epsilon_r^{sw}$$

$$\epsilon_\theta = \frac{1}{E}\left[\sigma_\theta - \mu(\sigma_r + \sigma_z)\right] + \alpha T + \epsilon_\theta^c + \epsilon_\theta^{gr} + \epsilon_\theta^{sw} + \Delta\epsilon_\theta^c + \Delta\epsilon_\theta^{gr} + \Delta\epsilon_\theta^{sw}$$

$$\epsilon_z = \frac{1}{E}\left[\sigma_z - \mu(\sigma_r + \sigma_\theta)\right] + \alpha T - \left(\epsilon_r^c + \epsilon_\theta^c + \epsilon_r^{gr} + \epsilon_\theta^{gr} + \epsilon_r^{sw} + \epsilon_\theta^{sw}\right)$$

$$- \left(\Delta\epsilon_\theta^c + \Delta\epsilon_r^c + \Delta\epsilon_\theta^{gr} + \Delta\epsilon_r^{gr} + \Delta\epsilon_\theta^{sw} + \Delta\epsilon_r^{sw}\right)$$

With each time increment the three incremental strains are defined, and convergence is obtained prior to the next increment.

Procedure for Calculations

The procedure for applying the creep analysis is as follows:

(1) The core is calculated for criticality or a k_{eff} commensurate with the desired excess reactivity.

(2) The integrated power shapes of (1) are used for making a temperature map of the core.

(3) The core temperature profile, material properties, and boundary forces are used for the plastic stress-strain analysis of reference 4.

(4) The output strains of (3) are used to adjust material densities (and subsequently macroscopic cross sections); new k_{eff} values are calculated (reactor hot).

(5) The output strains of (3) are used as a starting point for the creep analysis of reference 4.

(6) The output strains of (5) at any given time T are used to adjust material densities (and subsequent macroscopic cross sections); new k_{eff} values are calculated (reactor full power).

The calculations of (4) and (6) represent the k_{eff} of the core after heatup and after a predetermined time of full power running. These k_{eff} values are a result not only of thermal expansion but also of temperature gradients, changes in material properties, and boundary forces.

CALCULATION OF REFERENCE DESIGN

A reference design has been selected which serves a twofold purpose: (1) to demonstrate the analytical procedure outlined in the previous section and (2) to determine the reactivity of the fast reactor core of figure 1 at cold-critical, at hot - full power, and after a period of running at full power. The work accomplished in reference 16 was used as a guideline for establishing initial core geometry.

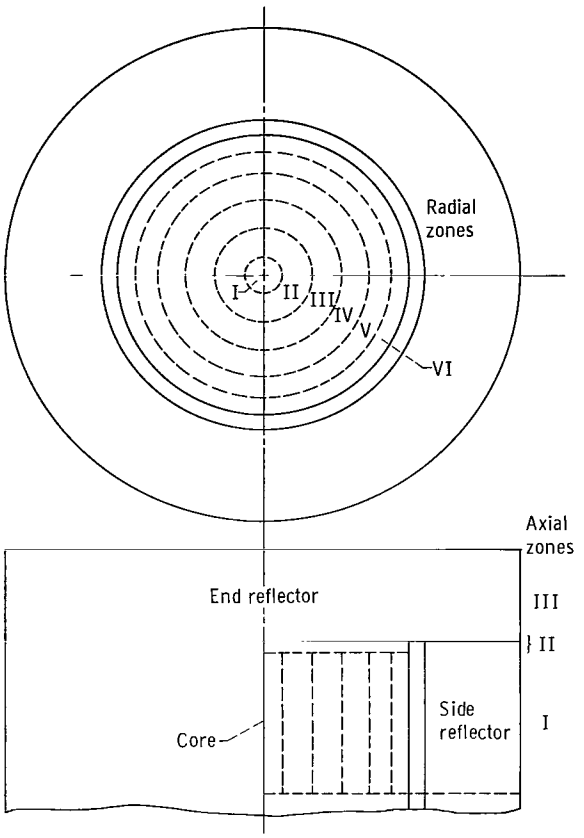

Figure 2. - Nuclear model.

A nuclear model of the core is illustrated in figure 2. The core is 12 inches (30.48 cm) in diameter by 12 inches (30.48 cm) long surrounded radially and axially by a 4-inch (10.16-cm) reflector. The assembly is made up of the following materials:

(1) Core - The fuel is fully enriched $U^{233}O_2$. Tungsten is used as a fuel carrier since its high melting point meets the requirements of a high-temperature core. The composition of the fuel cermet in volume percent is 40 $U^{233}O_2$ (full density), 50 tungsten, and 10 void.

(2) Coolant - Lithium is used as the liquid-metal coolant because of its good thermal properties and low neutron absorption cross section. It was assumed that the core consisted of 20 percent coolant.

(3) Expansion gap - This gap is filled with lithium which is displaced as core movement occurs.

(4) Reflector - Tungsten was chosen as a reflector. It was assumed that 5 percent of the reflector was lithium to provide reflector cooling.

Prior to the calculations of reactivity, the core was divided into seven radial zones and three axial zones (fig. 2 and tables I and II). These zones are subdivided into stations. Macroscopic cross sections and volumetric changes are considered to be constant throughout each zone.

TABLE I. - RADIAL ZONES AND STATIONS OF NUCLEAR MODEL

Station	Radius		Zone	Material	Region	Station	Radius		Zone	Material	Region
	in.	cm					in.	cm			
1	0.4	1.02	I	$W-UO_2$	Core	14	5.3	14.22	V	$W-UO_2$	Core
2	.8	2.03	I			15	5.5	14.73	V		
3	1.2	3.05	I			16	5.8	14.99	V		
4	1.6	4.06	II			17	6.0	15.24	V		
5	2.0	5.08	II			18	6.2	15.75	VI	Li	Expansion gap
6	2.4	6.10	II			19	6.4	16.26	VI	Li	Expansion gap
7	2.8	7.11	III			20	6.6	16.76	VI	Li	Expansion gap
8	3.2	8.18	III			21	7.4	18.80	VII	W	Reflector
9	3.6	9.14	III			22	8.2	20.83	VII		
10	4.0	10.16	IV			23	9.0	22.86	VII		
11	4.4	11.17	IV			24	9.8	24.89	VII		
12	4.8	12.19	IV			25	10.6	26.92	VII		
13	5.0	13.21	V								

TABLE II. - AXIAL ZONES AND STATIONS OF NUCLEAR MODEL

Station	Axial distance		Zone	Material	Region	Station	Axial distance		Zone	Material	Region
	in.	cm					in.	cm			
1	0.5	1.27	I	$W-UO_2$	Core	13	6.0	15.24	II	Li	Expansion gap
2	1.0	2.54				14	6.1	15.56	II	Li	Expansion gap
3	1.5	3.81				15	6.4	16.19	II	Li	Expansion gap
4	2.0	5.08				16	6.9	17.46	III	W	Reflector
5	2.5	6.35				17	7.4	18.43			
6	3.0	7.62				18	7.9	20.00			
7	3.5	8.89				19	8.4	21.27			
9	4.0	10.16				20	8.9	22.54			
10	4.5	11.43				21	9.4	23.81			
11	5.0	12.70				22	9.9	25.08			
12	5.5	13.97				23	10.4	26.35			

TABLE III. - NEUTRON ENERGY GROUPS

Group	Neutron energy range
1	2.23 to 14.9 MeV
2	0.82 to 2.23 MeV
3	185 to 820 KeV
4	40.7 to 185 KeV
5	5.55 to 40.7 KeV
6	0.76 to 5.55 KeV
7	0.414 to 760 eV

TABLE IV. - ATOM DENSITIES

Zone	Material	Region	Cold - critical	Hot - thermal stress	Hot - no stress
			Atom densities, atom/(cm)(b)		
I	U^{233}	Core	0.0077847	0.0075064	0.0075009
	O		.0155704	.0150137	.0150028
	W		.0252980	.0243930	.0243752
	Li		.0092719	.0092719	.0092719
II	U^{233}		0.0077847	0.0075073	0.0075026
	O		.0155704	.0150156	.0150062
	W		.0252980	.0243965	.0243811
	Li		.0092719	.0092719	.0092719
III	U^{233}		0.0077847	0.0075093	0.0075053
	O		.0155704	.0150196	.0150117
	W		.0252980	.0244029	.0243902
	Li		.0092719	.0092719	.0092719
IV	U^{233}		0.0077847	0.0075119	0.0075099
	O		.0155704	.0150247	.0150270
	W		.0252980	.0244113	.0244048
	Li		.0092719	.0092719	.0092719
V	U^{233}		0.0077847	0.0075151	0.0075151
	O		.0155704	.0150313	.0150313
	W		.0252980	.0244219	.0244219
	Li		.0092719	.0092719	.0092719
VI	Li	Expansion gap	0.0463595	No density change	No density change
VII	W	Reflector	0.0600828	No density change	No density change
	Li		.0023179		

Cold-Critical

The cold-critical state represents the core at the moment it has become critical and prior to any power generation. The macroscopic cross sections were calculated for the TDSN input. Seven group microscopic cross sections were used. The energy-group breakdown is shown in table III. The atom densities based on the core percentage composition used (32 $U^{233}O_2$, 40 W, 8 void) are shown in table IV. These values are used for converting the microscopic cross sections to macroscopic cross sections. The cross sections and the zone mesh points become part of the input to the TDSN program.

The resultant output for the cold-critical neutronic two-dimensional calculation was a k_{eff} of 1.0859 and the relative power distribution, as shown in figure 3. This case then represents the base line for reactivity comparison. The excess reactivity is typical of what would probably be designed into the core. The integrated power shapes can be used to calculate the core temperature map.

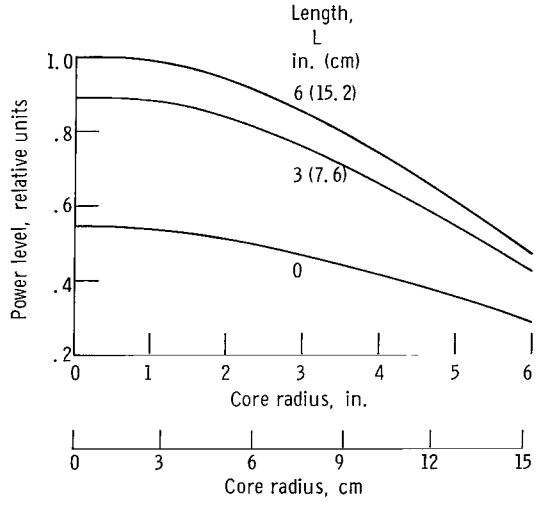

Figure 3. - Power level as function of core radius at core axial locations. Length is measured from cold end of core.

Hot - Full Power

As the core heats up to a full power condition, thermal growth $\alpha \Delta T$ takes place. The power shape is nonuniform, resulting in a temperature profile in the radial and axial direction. Core growth then becomes nonuniform. Consequently, thermal stresses incurred are superimposed on any existing stresses due to boundary and/or body forces.

The final core configuration is one in which original mesh points have now been displaced by the total strains.

For the hot - full power case, the integrated power shapes of the previous section (fig. 3) were converted into temperature profiles. This effort is outlined in appendix B. The maximum heat flux was not to exceed 2.0×10^6 Btu per hour per square foot (6.305 W/m^2), and the coolant inlet temperature was 2080° F (1411.1 K). This results in a temperature gradient in the fuel. The Δt is limited to less than 500° F (277.7 K). Maximum fuel temperature occurs midway between coolant passages. From preliminary experimental data on the thermal cycling of tungsten-UO_2 fuels (ref. 17), it appears that operation of this fuel material is feasible at these temperature gradients.

The thermal power generated by this core is approximately 10 megawatts. A typical coolant temperature rise is shown in figure 4 at a core radius of 0.8 inch (2.03 cm).

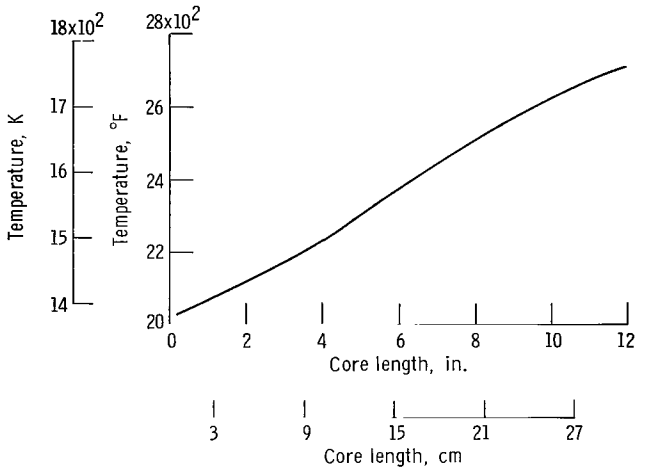

Figure 4. - Coolant temperature as function of core length at 0.8-inch (2.03-cm) radius.

The gross radial temperature gradient calculated becomes an input to the elastic-plastic calculation. This profile varies axially as does the power shape (see fig. 5). Station 14 (6.12 inches (15.54 cm) axially), which represents the point of maximum thermal stress, was selected to represent the core in the axial direction. The elastic stress-strain calculations were then made, and where the equivalent stress exceeds the yield a plastic stress-strain calculation is made.

As pointed out in reference 4, the plastic stress-strain analysis used the strain-strain method of solution. The stress-strain curve of figure 8(c) (appendix A) must be converted to an equivalent plastic strain - equivalent total strain curve through the equation

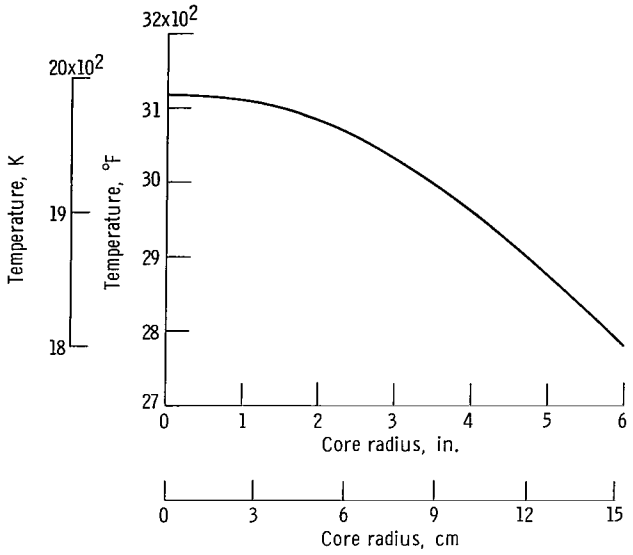

Figure 5. - Maximum metal temperature as function of core radius at station 14 (axial length, 6.12 in. (15.54 cm)).

$$\epsilon_{et} = \epsilon_p + \frac{2(1 + \mu)}{3} \frac{\sigma_e}{E}$$

The result is a strain-strain curve shown in figure 6. Yielding occurs when the equivalent total strain exceeds 0.00045 inch per inch (cm/cm).

To exemplify the above, both the elastic solution without the yield criteria applied and the elastic-plastic solution with the yield criteria applied were plotted. The elastic

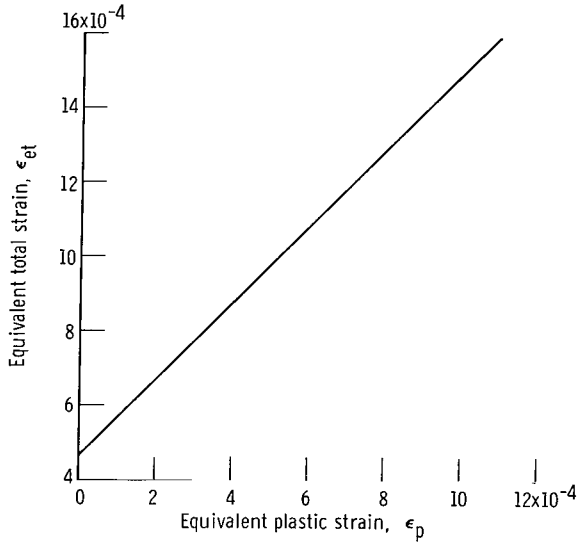

Figure 6. - Equivalent total strain as function of equivalent plastic strain at 3000° F (1922 K).

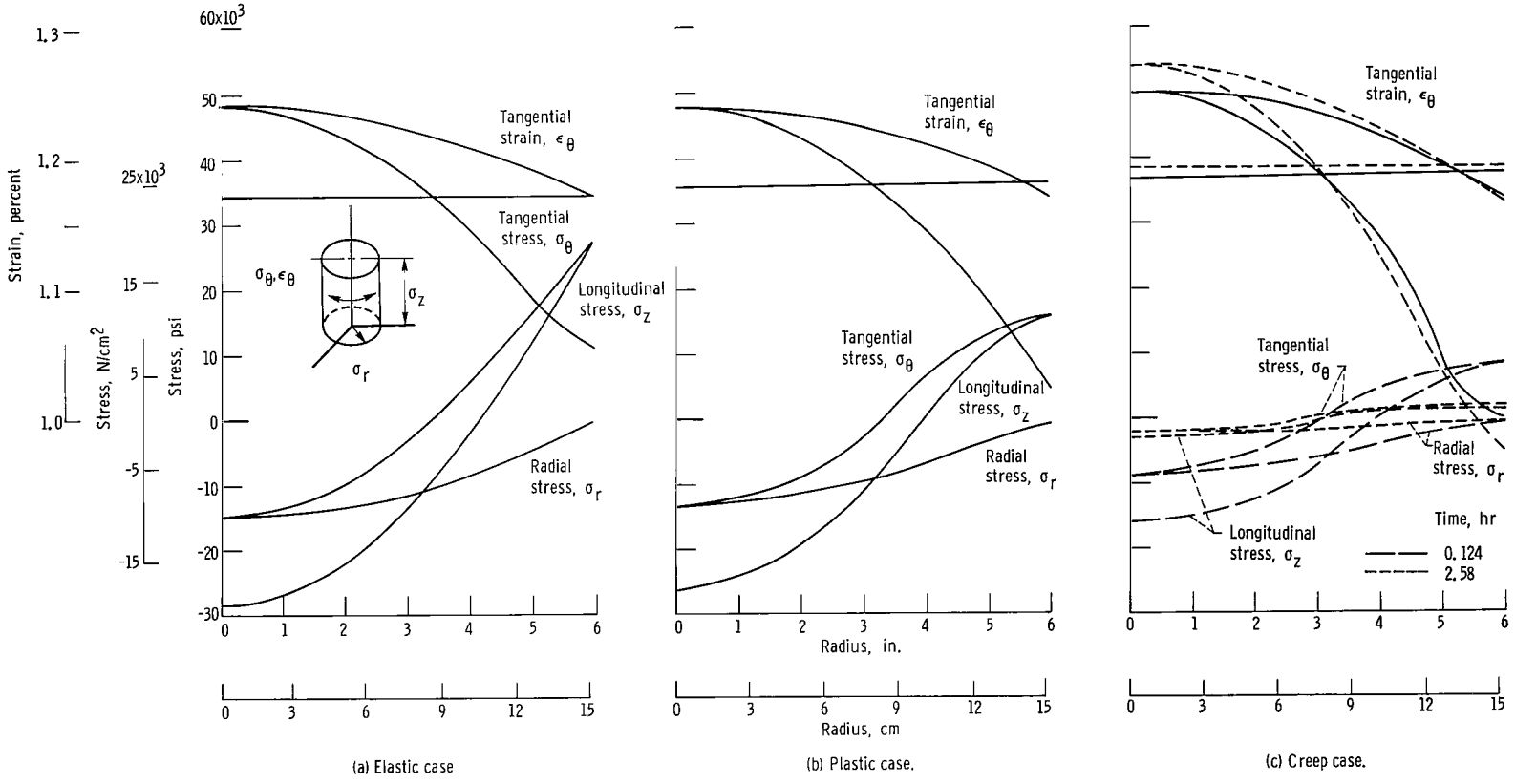

(a) Elastic case

(b) Plastic case.

(c) Creep case.

Figure 7. - Stress-strain as function of core radius.

solution is shown in figure 7(a), and the elastic-plastic solution is shown in figure 7(b). The σ_θ and σ_z stresses at the outer radius of the elastic solution were reduced from 30 000 psi (20 670 N/cm^2) to 15 000 psi (10 340 N/cm^2) since yielding took place from the 4.18-inch (10.62-cm) radius to the 6-inch (15.24-cm) radius. With yielding, however, changes are produced in the strains, which is evidenced by comparing the plots of ϵ_θ, ϵ_r, and ϵ_z in figures 7(a) and (b).

From a nucleonics point of view, these stresses represent a new position, since the radial mesh points after strain are related to the radial mesh points before strain by the equation

$$r_{new} = r_{old}(1 + \epsilon_\theta)$$

In addition, the longitudinal strain is related in a similar manner, with the reactor length resulting in a core volume change.

In table V, the radii of the radial mesh points for the case of a hot reactor are listed

TABLE V. - CORE VOLUME CHANGES

Station	Reactor cold	Reactor hot - thermal stress	Reactor hot - no stress	Reactor cold	Reactor hot - thermal stress	Reactor hot - no stress	Reactor hot, $(\Delta V/V)_1$	Stress relieved, $(\Delta V/V)_2$
	Length, in.			Length, cm				
	$L_0 = 1.0$	$L_1 = 1.01118$	$L_2 = 1.01210$	$L_0 = 2.54$	$L_1 = 2.56640$	$L_2 = 2.570734$		
	Radial station, in.			Radial station, cm			Volume change, percent	
	r_0	r_1	r_2	r_0	r_1	r_2		
1	0.40	0.404967	0.405057	1.016	1.028616	1.028845	3.708	0.074
2	.80	.809930	.810107	2.032	2.057220	2.057670	3.708	.073
3	1.20	1.214880	1.215130	3.048	3.085850	3.086430	4.120	.074
4	1.60	1.619800	1.620110	4.064	4.114290	4.115080	3.695	.068
5	2.00	2.024700	2.025040	5.080	5.142730	5.143600	3.682	.063
6	2.40	2.429500	2.429920	6.096	6.170930	6.172000	3.681	.064
7	2.80	2.834400	2.834710	7.112	7.199370	7.200160	3.668	.052
8	3.20	3.239110	3.239420	8.128	8.277340	8.228130	3.658	.049
9	3.60	3.643810	3.644040	9.144	9.255280	9.255860	3.645	.042
10	4.00	4.048440	4.043550	10.160	10.283040	10.283370	3.632	.036
11	4.40	4.453010	4.452950	11.176	11.310650	11.310490	3.617	.027
12	4.80	4.857480	4.857220	12.190	12.338000	12.337300	3.528	.020
13	5.04	5.100100	5.099700	12.800	12.594300	12.953240	3.589	.017
14	5.28	5.342680	5.342150	13.410	13.570410	13.569060	3.587	.011
15	5.52	5.585240	5.584570	14.020	14.186510	14.184810	3.587	.005
16	5.76	5.827760	5.826940	14.630	14.802510	14.800430	3.567	.005
17	6.00	6.070230	6.069260	15.240	15.418380	15.415920	3.563	.005

along with the change in volume $\Delta V/V$. The outside radius of the core increased by 1.18 percent, while the core length increased by 1.12 percent.

With the $\Delta V/V$ values the macroscopic cross sections of the five core zones are corrected (see table IV), and a new two-dimensional TDSN calculation is made. The reactivity of the core in the steady-state hot - full power condition is 1.07408, or a ΔK of -0.01182 (using a β of 0.00307). This represents a reactivity worth of - \$3.85. Most of this reactivity reflects the $\alpha \Delta T$ contribution since the core is heating up to 3000° F (1922 K).[1]

Ninety-Hour Full Power Operation - Creep

When the reactor is at a full power operating temperature of 3000° F (1922 K), creep of the core fuel metal takes place. The strains and temperature profile of the final solution of the elastic-plastic analysis now are the starting point for the creep calculations. These calculations were made at time increments of 0.01 hour. Figure 7(c) shows the stresses and strains at a total time of 0.124 and 2.58 hours. These plots show a rapid stress relaxation since at 0.124 hour the 15 000-psi (10 300-N/cm^2) longitudinal and tangential stress levels are already reduced to 8000 psi (5500 N/cm^2). At a total time of 2.58 hours, these same stresses are less than 2500 psi (1380 N/cm^2).

The strains plotted in figure 7(c) show the additional core movement that takes place as the thermal stresses relax. A time of 90 hours was chosen as the point in which all the thermal stresses had relaxed, and only the boundary stress of 500 psi (345 N/cm^2) applied by banding of the core remained in the core. As before, new radial and longitudinal positions of the mesh points (r_2L_2, table V) were converted into volume changes $(\Delta V/V)_2$. The total core axial length has changed by 1.21 percent, which is a slight increase over the hot-reactor situation. The outside radius, however, increased a total of 1.15 percent, which is slightly less than the hot-reactor situation and thus shows a decrease in core radius.

With the $(\Delta V/V)_2$ values the macroscopic cross sections for each zone were adjusted accordingly (table IV). A TDSN calculation was made, and the reactivity of the core after 90 hours of full power operation is 1.07388, or a ΔK of -0.00019. This is a reactivity worth of - \$0.06. Although this is a small amount of reactivity, most of it would occur during the first hour or two of operation. A second situation occurring is

---

[1]In an effort to evaluate reactivity changes due only to structural changes, the density of the lithium 7 (Li^7) coolant was held constant for all cases calculated. Actually, a density change of 20 percent can occur from the melting point to 3000° F (1922 K). For this reactor design this would be a negative reactivity of approximately \$0.80.

the effect of rapid relaxation on the problem of residual stresses. Although the local strains required to reduce the thermal stresses are very small, the cool fibers are stretched, and the hot fibers are shortened. Consequently, when the reactor is shut down, opposite stresses occur which are greater than the hot condition because of the higher elastic modulus at the lower temperatures. It appears that a fast-reactor design utilizing tungsten as a fuel carrier would suffer residual stresses in less than 1 hour of operation.

Two-Thousand-Hour Full Power Operation - Creep

With continued full power operation of the reactor at no thermal stresses, a compression of the core accompanied by a longitudinal increase will occur because of the 500-psi (345-N/cm^2) banded force used to contain the hexagonal fuel elements. After 2000 hours of reactor operation, new radial and longitudinal mesh points were recorded. The reactor length continued to grow, with a 1.69 percent increase relative to the original length; and the core radius decreased slightly from the 90-hour size, with a 1.09 percent increase relative to the original radius. With all thermal stresses relieved, the density of the core remained unchanged and in effect only a core length to diameter ratio is changed.

A calculation was made on TDSN using the new dimensions. The reactivity was 1.07374, or a ΔK of -0.00014. This represents a further decrease in reactivity of \$0.05 from the 90-hour calculation. It is considered negligible particularly since it would occur over 2000 hours of operation.

DISCUSSION OF RESULTS

The application of the elastic-plastic and creep analysis to reactor core changes was simple and effective. This method can be expanded to include irradiation swelling, irradiation growth, and reactor cycling. It will give core strains (and subsequent reactivity) based on the core's history of operation.

The core growth and subsequent reactivity changes were calculated for a constrained core. The growth and reactivity changes were small compared to the unconstrained cores of references 2 and 3. The reason for this is two-fold: (1) the bonds prevented fuel-element bowing; and (2) core changes were based on calculated structural strains, which were small radial and axial movements.

The primary contribution to the reactivity change results from the initial heating of the core. This is a volumetric change which is not uniform because of a temperature

TABLE VI. - RESULTS OF CALCULATION OF TOTAL AXIAL FLUID TEMPERATURE RISE

(a) U. S. Customary Units

Station	Radius, in.					
	0.8	2.0	3.2	4.4	5.28	6.0
	Total coolant temperature rise, $\Delta t'$, ^{o}F					
1	19	18	17	14	12	10
2	40	39	35	30	25	22
3	64	62	56	47	40	34
4	91	86	78	66	56	47
5	119	113	102	86	72	61
6	148	141	127	108	90	75
7	180	171	153	130	108	90
8	213	202	181	153	127	106
9	246	234	209	177	147	123
10	281	267	238	201	167	129
11	316	300	268	226	187	156
12	351	333	298	251	207	173
13	387	367	328	276	228	190
14	422	400	357	300	248	207
15	457	433	386	325	268	223
16	491	464	415	349	288	240
17	523	495	442	372	307	255
18	555	525	469	394	325	271
19	585	553	494	415	343	285
20	613	580	518	435	359	299
21	639	605	540	454	375	312
22	663	628	561	472	389	324
23	684	648	579	487	403	336
24	704	666	596	502	415	346

(b) SI Units

Station	Radius, cm					
	2.03	5.08	8.13	11.18	13.41	15.24
	Total coolant temperature rise, $\Delta t'_f$, K					
1	11	10	9	8	7	6
2	22	22	19	17	14	12
3	36	34	31	26	22	19
4	51	48	43	37	31	26
5	66	63	57	48	40	34
6	82	78	71	60	50	42
7	100	95	85	72	60	50
8	118	112	101	85	71	59
9	137	130	116	98	82	68
10	156	148	132	112	93	77
11	176	167	149	126	104	87
12	195	185	166	139	115	96
13	215	204	182	153	127	106
14	234	222	198	167	138	115
15	254	241	214	181	149	124
16	273	258	231	194	160	133
17	291	275	246	207	171	142
18	308	292	261	219	181	151
19	325	307	274	231	191	158
20	341	322	288	242	199	166
21	355	336	300	252	208	173
22	368	349	312	262	216	180
23	380	360	322	271	224	187
24	391	370	331	279	231	192

gradient in the radial and axial directions. Table VI lists the radial and axial mesh point dimensions for each station at the conditions of reactor cold, reactor hot - thermal stress, and reactor hot - no stress. The nonuniformity in the expansion of the radial mesh points is also reflected by the tangential strain ϵ_θ plotted in figures 7(b) and (c). The bending of the curve in the radial direction represents the nonuniform expansion of the core. It is difficult to predict the performance of the core for all reactor designs since ϵ_θ is affected by the temperature gradient across the core, the fuel thermal coefficient of expansion, and the modulus of elasticity.

Continued operation of the core results in small changes in reactivity when the individual fuel elements are banded together and the core performs as a homogeneous cylinder. During this operation phase, the primary contribution to reactivity changes is the creep strain. Again, the magnitude of the reactivity change is a result of the creep strains which are affected by the fuel material, radial temperature gradients, and the temperature level of operation.

An observation made during the analysis was the sudden relaxation of the stresses during the creep phase (fig. 7(c)). During the first few hours of reactor operation the stresses relaxed almost to their asymptotic values. Reactor shutdown occurring after this period would result in a buildup of opposite stresses which become greater because of the change of values of the modulus of elasticity. The high operating temperature of the tungsten and the resultant creep strain are the primary reasons for the rapid relaxation of stresses.

CONCLUSIONS

The method of successive approximations for calculating the plastic stresses and strains in a core proved to be effective. This method can be expanded to include irradiation swelling, irradiation growth, and reactor cycling. It will give core strains (and subsequent reactivity) based on the core's history of operation.

In applying this analysis to a 10-megawatt tungsten-reflected core 12 inches (30.48 cm) in diameter by 12 inches (30.48 cm) long with tungsten $U^{233}O_2$ as the fuel, the following observations were made:

1. A heatup reactivity decrease of - $3.85 occurred, which is common for fast reactors of this size and type of fuel.

2. After initial heatup of the core, the reactivity changes were small and of the order of - $0.06 for 90 hours and - $0.05 for 90 to 2000 hours.

3. A rapid relaxation of thermal stresses occurs during the fuel power operation of the reactor because of creep. A fast reactor utilizing tungsten as a fuel carrier would suffer high residual stresses at chilldown in approximately 1 hour of operation.

4. When fuel elements are bundled to prevent individual bowing, the strains of the core do not cause large reactivity changes during the operation of the reactor.

Lewis Research Center,
National Aeronautics and Space Administration,
Cleveland, Ohio, October 3, 1968,
126-15-01-03-22.

APPENDIX A

PROPERTY DATA

The data contained in this appendix are from the personal notes of Mr. R. Buzzard of Lewis Research Center. Most of the data represent work conducted over the past 4 years on tungsten fueled with uranium dioxide (table VII; figs. 8 and 9).

TABLE VII. - CREEP RUPTURE PROPERTIES OF TUNGSTEN - 20 PERCENT UO_2

Test temperature		Initial stress		Creep rate, in./in./min (cm/cm/min)
^{o}F	K	psi	N/cm^2	
3000	1922	2220	1530	1.0×10^{-6}
		2500	1720	7.0×10^{-7}
		3000	2065	2.0×10^{-6}
		4000	2750	8.0
		6000	4130	1.2×10^{-5}
		7000	4820	1.4
		9000	6200	3.8
3500	2200	2220	1530	923
		2500	1720	528
		3000	2065	293
		4000	2750	165

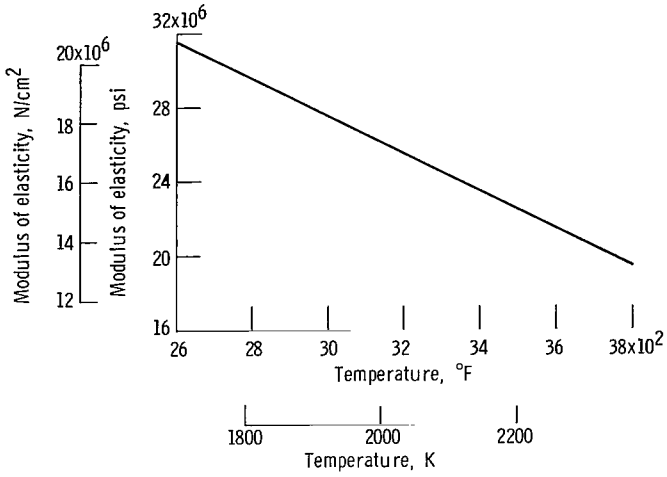

(a) Elastic modulus of tungsten at high temperatures.

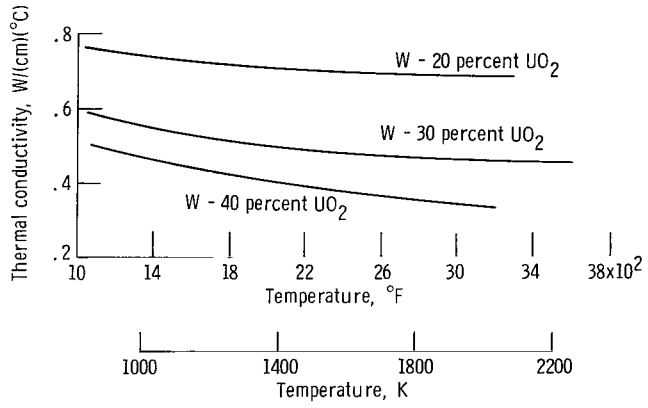

(b) Thermal conductivity as function of temperature.

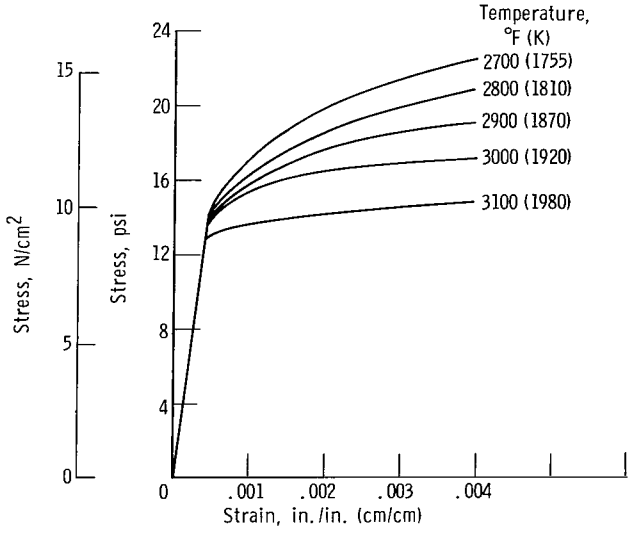

(c) Stress as function of strain for tungsten.

Figure 8. - Properties of tungsten and tungsten UO$_2$.

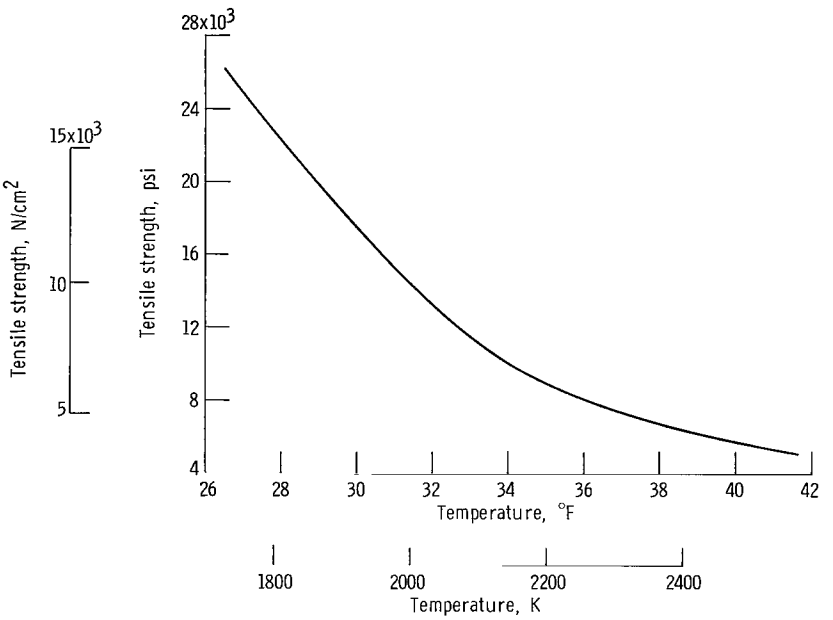

Figure 9. - Ultimate tensile strength as function of temperature for tungsten - 20-volume-percent UO_2.

APPENDIX B

HEAT-TRANSFER ANALYSIS

The heat-transfer analysis pertains to the dissipation of the heat of the reactor core to the coolant fluid passing through the core. The modes of heat transfer considered were heat conduction due to internal heat generation from the fuel material (tungsten-UO_2) to the coolant passage walls, heat convection from the walls to the bulk fluid, and finally the gain in heat of the bulk fluid as it passes through the core. The equations used are outlined in the following sections:

Geometric Equations

$$\text{Cross-sectional area of one hexagonal fuel element} = 2.59808\ S^2 \qquad \text{(B1)}$$

Where $S = 0.28868$ (see fig. 10), the area is 0.21651 square inch (1.3965 cm^2).

$$\text{Area of coolant (20 percent)} = 0.2 \times \text{Area of hexagonal fuel element}$$

$$= 0.0433028\ \text{in.}^2\ (0.27928\ cm^2) \qquad \text{(B2)}$$

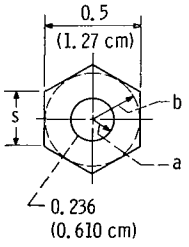

Figure 10. - Tungsten-UO_2 fuel element 20-volume-percent coolant fraction.

$$\text{Diameter of coolant holes} = \sqrt{\frac{4}{\pi}} \times \text{Area of coolant passage}$$

$$= 0.235 \text{ in. } (0.5969 \text{ cm}) \tag{B3}$$

Convection Equations

In a study of liquid metals, Lubarsky and Kaufman (ref. 18) found that the emperical equation

$$Nu = 0.625\left(Re_d Pr\right)^{0.4} \tag{B4}$$

correlates most constant heat flux data in the fully developed turbulent flow regime

$$h = 0.625 \frac{K}{d}\left(\frac{\rho V d}{\mu_1} \frac{C_p \mu_1}{K}\right)^{0.4} \tag{B5}$$

where $C_p = 1.0$ and $d = 0.236$ inch (0.599 cm). Then

$$h = 6.60\, K^{0.6} \rho^{0.4} V^{0.4} \tag{B6}$$

The heat transfer across the film is

$$Q = hA(t_a - t_f) \tag{B7}$$

Conduction Equations

The equation of conduction when expressed in cylindrical coordinates becomes (ref. 19)

$$\frac{1}{r} \frac{\partial}{\partial r}\left(r \frac{\partial t}{\partial r}\right) + \frac{1}{r^2} \frac{\partial^2 t}{\partial \theta^2} + \frac{\partial^2 t}{\partial z^2} = \frac{1}{K} \frac{\partial t}{\partial T} \tag{B8}$$

For heat production in a cylinder whose axis coincides with the axes of Z, and for which boundary conditions are independent of the coordinates θ and Z, the temperature

is a function of r and T only. For steady state, the equation further reduces to

$$\frac{1}{r}\frac{d}{dr}\left(r\frac{dt}{dr}\right)+\frac{A_0}{K}=0 \tag{B9}$$

which upon integration reduces to

$$\frac{dt}{dr}=-\frac{A_0 r}{2K}+C_1 \tag{B10}$$

and

$$t=-\frac{A_0 r}{2K}+C_2 \tag{B11}$$

For the solution of C_1 and C_2 the boundary conditions of $(dt/dr)_{r=b}=0$ and $t=t_a$ at $r=a$ are used. The final answer becomes

$$t_b-t_a=\frac{A_0}{2K}\left[\frac{a^2}{2}+b^2\left(\log\frac{b}{a}-\frac{1}{2}\right)\right] \tag{B12}$$

which is the temperature drop in the fuel from the maximum t_b to the coolant wall t_a.

For the temperature gradient at the coolant wall, equation (B10) at $r=a$ becomes

$$\frac{dt}{dr}=-\frac{A_0}{2K}\left(a-\frac{b^2}{a}\right) \tag{B13}$$

since

$$K\left(\frac{dt}{dr}\right)_{r=a}=\frac{Q}{A}\bigg|_{r=a}$$

Therefore,

$$t_a-t_f=\frac{A_0}{2h}\left(\frac{b^2}{a}-a\right) \tag{B14}$$

and, thus, the temperature drop from the maximum fuel temperature to the bulk fluid is (ref. 20)

$$t_b - t_f = \frac{A_0}{2K}\left[\frac{a^2}{2} + b^2\left(\log \frac{b}{a} - \frac{1}{2}\right)\right] + \frac{A_0}{2h}\left(\frac{b^2}{a} - a\right) \tag{B15}$$

Coolant-Channel Thermal Equations

The rate ΔQ at which heat is added to the coolant stream in an incremental length ΔX is given by

$$\Delta Q = WC_p\, \Delta t' \tag{B16}$$

where $\Delta t'$ is the differential temperature increase in the coolant in the length ΔX. This heat gain is transferred from the fuel element to the liquid in a ΔX length at a heat flux of Q/A. The heat rate ΔQ is equated to the heat flux by the relation

$$\left.\begin{aligned} \Delta Q &= \frac{Q}{A} \times \text{Area of an element} \\ \text{or} \qquad \Delta Q &= \frac{Q}{A}\, \pi d\, \Delta X \end{aligned}\right\} \tag{B17}$$

For $d = 0.236$ inch (0.599 cm) and $\Delta X = 0.5$ inch (1.27 cm),

$$\Delta Q = 0.002575\, \frac{Q}{A} \tag{B18}$$

Finally, combining equations (B16) and (B18) and assuming coolant velocities of 5 feet per second (1.524 m/sec) at a density of 28.5 pounds per cubic foot (456.5 kg/m^3) and a C_p of 1.0 results in

$$\Delta t' = \frac{Q}{A} \times 1.78 \times 10^{-5} \tag{B19}$$

For each increment along the channel

$$\Delta t_i' = \left(\frac{Q}{A}\right)_i \times 1.78\times10^{-5} \tag{B20}$$

Where Q/A takes on a new value for each increment i. The coolant temperature rise across the core at radius r is thus

$$\Delta t'\Big|_{\text{radius=r}} = \sum_{i=1}^{n} \Delta t_i' \tag{B21}$$

$$\Delta t'\Big|_{\text{radius=r}} = 1.78\times10^{-5} \sum_{i=1}^{n} \left(\frac{Q}{A}\right)_i \tag{B22}$$

where n is the number of increments along the core length.

Core Temperature Distribution

Using these equations the coolant temperature and the fuel metal temperature can be calculated for each axial station from i = 1, . . ., n. To provide the core temperature distribution, the power ratios in the radial direction at various increments along the core axis, as available from the TDSN code, are used to adjust the heat-flux values $(Q/A)_i$. A heat flux of 2.0×10^6 Btu per hour per square foot (6.3×10^6 W/m^2) was assumed to exist at the maximum power ratio of 1. As the power decreases both axially and radially, the heat flux was adjusted proportionately. When $(Q/A)_i$ at stations i - 1, . . ., n is known, the Δt can be computed from equation (B22). The results of those calculations are presented in table VIII for axial increments i = 1, . . ., 24 at radial locations of 0.8, 2.0, 3.2, 4.4, 5.28, and 6.0 inches (1.232, 5.08, 8.13, 11.18, 13.46, and 15.24 cm).

From the results of table VIII, the fluid temperature rise $\Delta t'$ in the axial direction at the aforementioned radial locations can be calculated by using equation (B21). The results of these calculations are presented in table VI.

Finally, when a radially constant coolant temperature entering the core of 2030° F (1383.3 K) is assumed, the fluid temperature and the maximum fuel metal temperature can be calculated by using equations (B12), (B14), and (B15). These results are presented in table IX.

TABLE VIII. - RESULTS OF CALCULATION OF INCREMENTAL AXIAL FLUID TEMPERATURE INCREASE

(a) U.S. Customary Units

Station[a]	Radius, in.																	
	0.8			2.0			3.2			4.4			5.28			6.0		
	Power level	Heat flux, $(Q/A)_i$, Btu/(hr)(ft^2)	Total coolant temperature rise, $\Delta t'_i$, °F	Power level	Heat flux, $(Q/A)_i$, Btu/(hr)(ft^2)	Total coolant temperature rise, $\Delta t'_i$, °F	Power level	Heat flux, $(Q/A)_i$, Btu/(hr)(ft^2)	Total coolant temperature rise, $\Delta t'_i$, °F	Power level	Heat flux, $(Q/A)_i$, Btu/(hr)(ft^2)	Total coolant temperature rise, $\Delta t'_i$, °F	Power level	Heat flux, $(Q/A)_i$, Btu/(hr)(ft^2)	Total coolant temperature rise, $\Delta t'_i$, °F	Power level	Heat flux, $(Q/A)_i$, Btu/(hr)(ft^2)	Total coolant temperature rise, $\Delta t'_i$, °F
1	0.545	1.090	19	0.517	1.034	18	0.467	0.934	17	0.399	0.798	14	0.339	0.678	12	0.290	0.580	10
2	.608	1.216	22	.579	1.158	21	.522	1.044	19	.446	.892	16	.376	.752	13	.316	.632	11
3	.674	1.349	24	.639	1.278	23	.575	1.150	20	.489	.978	17	.408	.816	15	.342	.684	12
4	.734	1.468	26	.696	1.392	25	.626	1.250	22	.530	1.060	19	.439	.878	16	.367	.734	13
5	.789	1.580	28	.748	1.496	27	.668	1.336	24	.566	1.132	20	.467	.934	17	.390	.780	14
6	.839	1.680	30	.796	1.592	28	.711	1.420	25	.598	1.196	21	.494	.988	18	.411	.822	15
7	.881	1.760	31	.839	1.678	30	.748	1.500	27	.626	1.252	22	.516	1.032	18	.429	.858	15
8	.921	1.840	33	.869	1.738	31	.772	1.540	28	.650	1.300	23	.535	1.070	19	.445	.890	16
9	.948	1.900	34	.899	1.798	32	.802	1.604	29	.669	1.340	24	.551	1.102	20	.458	.916	16
10	.973	1.950	35	.920	1.840	33	.821	1.640	29	.687	1.370	24	.563	1.126	20	.467	.934	17
11	.988	1.980	35	.934	1.868	33	.833	1.665	30	.696	1.390	25	.571	1.142	20	.474	.948	17
12	.996	1.990	35	.941	1.880	33	.839	1.678	30	.699	1.400	25	.575	1.150	20	.477	.954	17

(b) SI Units

Station[a]	Radius, cm																	
	2.03			5.08			8.13			11.18			13.41			15.24		
	Power level	Heat flux, $(Q/A)_i$, W/m^2	Total coolant temperature rise, $\Delta t'_i$, K	Power level	Heat flux, $(Q/A)_i$, W/m^2	Total coolant temperature rise, $\Delta t'_i$, K	Power level	Heat flux, $(Q/A)_i$, W/m^2	Total coolant temperature rise, $\Delta t'_i$, K	Power level	Heat flux, $(Q/A)_i$, W/m^2	Total coolant temperature rise, $\Delta t'_i$, K	Power level	Heat flux, $(Q/A)_i$, W/m^2	Total coolant temperature rise, $\Delta t'_i$, K	Power level	Heat flux, $(Q/A)_i$, W/m^2	Total coolant temperature rise, $\Delta t'_i$, K
1	0.545	3.430	10.6	0.517	3.260	10.0	0.467	2.944	9.4	0.399	2.516	7.8	0.339	2.137	6.7	0.290	1.828	5.6
2	.608	3.833	12.2	.579	3.651	11.7	.522	3.291	10.6	.446	2.812	8.9	.376	2.371	7.2	.316	1.992	6.1
3	.674	4.253	13.3	.639	4.029	12.8	.575	3.625	11.1	.489	3.083	9.4	.408	2.572	8.3	.342	2.156	6.7
4	.734	4.628	14.4	.696	4.388	13.9	.626	3.940	12.2	.530	3.341	10.6	.439	2.768	8.9	.367	2.314	7.2
5	.789	4.981	15.6	.748	4.716	15.0	.668	4.212	13.3	.566	3.569	11.1	.467	2.944	9.4	.390	2.459	7.8
6	.839	5.206	16.7	.796	5.019	15.6	.711	4.477	13.9	.598	3.770	11.7	.494	3.115	10.0	.411	2.591	8.3
7	.881	5.548	17.2	.839	5.290	16.7	.748	4.729	15.1	.626	3.947	12.2	.516	3.253	10.0	.429	2.705	8.3
8	.921	5.800	18.3	.869	5.479	17.2	.772	4.855	15.6	.650	4.098	12.8	.535	3.373	10.6	.445	2.806	8.9
9	.948	5.990	18.9	.899	5.668	17.8	.802	5.057	16.1	.669	4.224	13.3	.551	3.474	11.1	.458	2.888	8.9
10	.973	6.147	19.4	.920	5.800	18.3	.821	5.170	16.1	.687	4.319	13.3	.563	3.550	11.1	.467	2.944	9.4
11	.988	6.242	19.4	.934	5.889	18.3	.833	5.249	16.7	.696	4.382	13.9	.571	3.600	11.1	.474	2.990	9.4
12	.996	6.273	19.4	.941	5.927	18.3	.839	5.290	16.7	.699	4.413	13.9	.575	3.625	11.1	.477	3.007	9.4

[a]Stations 13 to 24 are symmetrical with stations 1 to 12.

TABLE IX. - RESULTS OF THE CALCULATION OF MAXIMUM METAL TEMPERATURE

(a) U. S. Customary Units

Station	Radius, in.											
	0.8		2.0		3.2		4.4		5.28		6.0	
	Temperature, ^{o}F											
	At film	At radius b	At film	At radius b	At film	At radius b	At film	At radius b	At film	At radius b	At film	At radius b
13	2417	3084	2397	3049	2358	2985	2306	2890	2258	2810	2220	2745
[a]14	2452	3116	2430	3078	2387	3017	2330	2921	2278	2841	2237	2776
15	2487	3139	2463	3105	2416	3044	2355	2952	2298	2872	2253	2808
16	2521	3158	2494	3123	2445	3066	2379	2975	2318	2899	2270	2834
17	2553	3171	2525	3136	2472	3076	2402	2995	2337	2919	2285	2858
18	2585	3176	2555	3150	2499	3085	2424	3008	2355	2940	2301	2879
19	2615	3176	2584	3149	2524	3096	2445	3019	2373	2955	2315	2897
20	2642	3172	2610	3145	2548	3096	2465	3027	2389	2963	2329	2909
21	2669	3161	2635	3138	2570	3092	2484	3028	2405	2970	2342	2920
22	2693	3147	2658	3124	2591	3082	2502	3025	2419	2971	2354	2925
23	2714	3122	2678	3103	2609	3069	2517	3015	2433	2970	2366	2931
24	2734	3100	2696	3081	2626	3050	2532	3005	2445	2966	2376	2932

(b) SI Units

Station	Radius, cm											
	2.03		5.08		8.13		11.18		13.41		15.24	
	Temperature, K											
	At film	At radius b	At film	At radius b	At film	At radius b	At film	At radius b	At film	At radius b	At film	At radius b
13	1598	1969	1587	1949	1566	1914	1537	1861	1510	1817	1489	1781
[a]14	1618	1987	1606	1966	1582	1932	1550	1878	1521	1834	1498	1792
15	1637	1999	1624	1964	1598	1947	1564	1896	1532	1851	1507	1816
16	1656	2010	1641	1991	1614	1959	1577	1908	1543	1866	1517	1830
17	1674	2017	1658	1998	1629	1964	1580	1919	1554	1877	1525	1843
18	1692	2020	1675	2006	1643	1969	1602	1927	1564	1889	1534	1855
19	1708	2020	1691	2005	1658	1976	1614	1933	1574	1897	1542	1865
20	1723	2018	1706	2003	1671	1976	1625	1937	1583	1902	1549	1872
21	1738	2012	1719	1999	1683	1973	1636	1938	1592	1906	1557	1878
22	1752	2004	1732	1991	1695	1968	1646	1936	1599	1906	1563	1881
23	1763	1990	1743	1979	1705	1961	1654	1931	1607	1906	1570	1884
24	1774	1978	1753	1967	1714	1950	1662	1925	1614	1900	1572	1884

[a]Station chosen for stress-strain and creep analysis.

APPENDIX C

STRESS-STRAIN - TIME RELATIONS

On the basis of data available for tungsten-UO_2, the constant-temperature stress-strain - time relation was chosen. It is one in which the logarithm of the linear creep rate against the logarithm of stress is linear. Thus,

$$\log \dot{\epsilon} = \log A_1 + N \log \sigma \tag{C1}$$

or

$$\dot{\epsilon} = A_1 \sigma^N \tag{C2}$$

where the values of N and A are based on the data available. To obtain unique values for these constants the least-squares procedure was applied.

A residual R is defined as

$$R = \log \dot{\epsilon} - \log \dot{\epsilon}' \tag{C3}$$

where $\log \dot{\epsilon}$ is the logarithm of the experimentally measured value of the linear creep rate and $\dot{\epsilon}'$ is the logarithm of the linear creep rate value using equation (C1).

Combining equations (C1) and (C3) and taking the sum gives

$$\sum (R)^2 = \sum (\log \dot{\epsilon} - \log A_1 - N \log \sigma)^2 \tag{C4}$$

Differentiating with respect to $\log A_1$ and setting the result equal to zero to find the minimum give

$$\sum_{i=1}^{J} \log \dot{\epsilon} = J \log A_1 + N \sum_{i=1}^{J} \log \sigma \tag{C5}$$

Now differentiating with respect to N and setting the result equal to zero give

$$\sum_{i=1}^{J} \log \dot{\epsilon} \log \sigma = \log A_1 \sum_{i=1}^{J} \log \sigma + N \sum_{i=1}^{J} \log^2 \sigma \tag{C6}$$

When performing the proper summation operation with the experimental data, equations (C5) and (C6), when solved simultaneously, will yield the unique values N and A_1.

Equation (C2) then becomes in finite difference form

$$\Delta\epsilon = A_1 \sigma_e^N \Delta T \tag{C7}$$

or

$$\Delta\epsilon_{ec} = A_1 \sigma_e^N \Delta T \tag{C8}$$

When the data of table VII are used, this equation becomes, at 3000° F (1922 K),

$$\Delta\epsilon_{ec} = 1.7 \times 10^{-12} \sigma_e^{2.27} \Delta T \tag{C9}$$

REFERENCES

1. Thalgott, F. W.; Boland, J. F.; Brittan, R. O.; Carter, J. C.; McGinnis, F. D.; Novick, M.; Okrent, D.; Sandmeier, H. A.; Smith, R. R.; and Rice, R. E.: Stability Studies on EBR-1. Reactor Physics. Vol. 12 of the Proceedings of the Second United Nations International Conference on the Peaceful Uses of Atomic Energy. United Nations, 1958, pp. 242-266.

2. Gronross, H.; and Davis, J. P.: Reactivity Effects from Fuel Displacement in a Small Thermionic Reactor. Space Programs Summary No. 37-45, Vol. IV. Rep. JPL-SPS-37-45, vol. IV, Jet Propulsion Lab., California Inst. Tech. (NASA CR-87450), June 30, 1967, pp. 136-141.

3. Sullivan, Robert E.: Reactivity Insertions in Compact Reactor Cores Due to Fuel Movement. NASA TM X-1587, 1968.

4. Puthoff, Richard L.: A Digital Computer Program for Determining the Elastic-Plastic Deformation and Creep Strains in Cylindrical Rods, Tubes and Vessels. NASA TM X-1723, 1968.

5. Meghreblian, Robert V.; and Holmes, David K.: Reactor Analysis. McGraw-Hill Book Co., Inc., 1960, p. 154.

6. Meneghetti, David: Introductory Fast Reactor Physics Analysis. Rep. ANL-6809, Argonne National Lab., Dec. 1963.

7. Barber, Clayton E.: A Fortran IV Two-Dimensional Discrete Angular Segmentation Transport Program. NASA TN D-3573, 1966.

8. Joanou, G. D.; and Dudek, J. S.: Gam-II. A B_3 Code for the Calculation of Fast-Neutron Spectra and Associated Multigroup Constants. Rep. GA-4265, General Atomic Div., General Dynamics Corp., Sept. 16, 1963.

9. Millenson, M. B.; and Manson, S. S.: Determination of Stresses in Gas-Turbine Disks Subjected to Plastic Flow and Creep. NACA TN 1636, 1948.

10. Johnson, Donald F.: Analysis of Elastic-Plastic Stress Distribution in Thin-Wall Cylinders and Spheres Subjected to Internal Pressure and Nuclear Radiation Heating. NASA TN D-371, 1960.

11. Yalch, J. P.: DEFCOT: Plane-Strain Plastic-Viscoelastic Deformation of a Composite Tube. Rep. GEMP-415, General Electric Co., June 1966.

12. Manson, S. S.: Thermal Stress and Low-Cycle Fatigue. McGraw-Hill Book Co., Inc., 1966.

13. Mendleson, A.; Herschberg, M. H.; and Manson, S. S.: A General Approach to the Practical Solution of Creep Problems. J. Basic Eng., vol. 81, no. 4, Dec. 1959, pp. 585-598.

14. Conway, J. B.: Properties of Some Refractory Metals. V. Numerical Methods for Creep and Rupture Analysis. Rep. GEMP-397, General Electric Co., Jan. 31, 1966.

15. Ma, Benjamin M.; and Murphy, Glenn: Radiation and Creep Analysis of Strains and Stresses in Annular Fuel Elements. Nucl. Structure Eng., vol. 1, 1965, pp. 141-154.

16. Lahti, Gerald P.; Lantz, Edward; and Miller, John V.: Preliminary Considerations for a Fast-Spectrum, Liquid-Metal Cooled Nuclear Reactor Program for Space-Power Applications. NASA TN D-4315, 1968.

17. Fiero, Ivan B.: Establishing Allowable Temperature Gradients for Tungsten-Uranium Dioxide Fuel Elements Using Experimental Cyclic Strain Data. NASA TN D-4279, 1968.

18. Lubarsky, Bernard; and Kaufman, Samuel J.: Review of Experimental Investigations of Liquid-Metal Heat Transfer. NACA TN 3336, 1955.

19. Kreith, Frank: Principles of Heat Transfer. Second ed., International Textbook Co., 1965.

20. Glasstone, Samuel: Principles of Nuclear Reactor Engineering. D. Von Nostrand Co., Inc., 1955.

NASA-Langley, 1969 —— 22 E-4280

NATIONAL AERONAUTICS AND SPACE ADMINISTRATION
WASHINGTON, D.C. 20546

OFFICIAL BUSINESS

FIRST CLASS MAIL

POSTAGE AND FEES PAID
NATIONAL AERONAUTICS AND
SPACE ADMINISTRATION

"The aeronautical and space activities of the United States shall be conducted so as to contribute . . . to the expansion of human knowledge of phenomena in the atmosphere and space. The Administration shall provide for the widest practicable and appropriate dissemination of information concerning its activities and the results thereof."

—NATIONAL AERONAUTICS AND SPACE ACT OF 1958

NASA SCIENTIFIC AND TECHNICAL PUBLICATIONS

TECHNICAL REPORTS: Scientific and technical information considered important, complete, and a lasting contribution to existing knowledge.

TECHNICAL NOTES: Information less broad in scope but nevertheless of importance as a contribution to existing knowledge.

TECHNICAL MEMORANDUMS: Information receiving limited distribution because of preliminary data, security classification, or other reasons.

CONTRACTOR REPORTS: Scientific and technical information generated under a NASA contract or grant and considered an important contribution to existing knowledge.

TECHNICAL TRANSLATIONS: Information published in a foreign language considered to merit NASA distribution in English.

SPECIAL PUBLICATIONS: Information derived from or of value to NASA activities. Publications include conference proceedings, monographs, data compilations, handbooks, sourcebooks, and special bibliographies.

TECHNOLOGY UTILIZATION PUBLICATIONS: Information on technology used by NASA that may be of particular interest in commercial and other non-aerospace applications. Publications include Tech Briefs, Technology Utilization Reports and Notes, and Technology Surveys.

Details on the availability of these publications may be obtained from:

SCIENTIFIC AND TECHNICAL INFORMATION DIVISION

NATIONAL AERONAUTICS AND SPACE ADMINISTRATION

Washington, D.C. 20546